
Metabolite Considerations in the In Vivo Quantification of Serotonin Transporters Using ^{11}C -DASB and PET in Humans

Ramin V. Parsey^{1,2}, Ashish Ojha², R. Todd Ogden³, Kjell Erlandsson^{1,4}, Dileep Kumar², Marguerite Landgrebe², Ronald Van Heertum^{2,4}, and J. John Mann^{1,4}

¹Department of Psychiatry, Columbia University College of Physicians and Surgeons, New York, New York; ²Department of Neuroscience, New York State Psychiatric Institute, New York, New York; ³Department of Biostatistics, Columbia University School of Public Health, New York, New York; and ⁴Department of Radiology, Columbia University College of Physicians and Surgeons, New York, New York

PET studies of the serotonin (5-hydroxytryptamine, or 5-HT) transporter are increasingly using ^{11}C -3-amino-4-(2-dimethylaminomethylphenylsulfanyl)benzotrile (DASB). We noted that the percentage of unmetabolized ^{11}C -DASB is often lower at 2 min after injection than at 12 min. We hypothesized that this is due to initial "trapping" of the unmetabolized ^{11}C -DASB compound in the lung, a major 5-HT transporter site and dose-limiting organ. To determine whether binding to an extracranial pool of 5-HT transporters contributes to the lower initial level of unmetabolized ^{11}C -DASB, we examined the effects of sertraline. **Methods:** Eleven healthy volunteers had 2 ^{11}C -DASB PET scans on the same day, and 6 of the 11 had a third scan after sertraline administration. The unmetabolized ^{11}C -DASB fraction was measured in arterial plasma as a function of time and was fit with 2 exponentials with no damping, power function damping, or no damping with the first point removed. **Results:** Power function damping best fit the data as assessed by visual inspection and residuals and resulted in greater distribution volumes than did no damping with the first point removed. Test-retest reproducibility improved when power function damping was used, as compared with no damping with the first point removed. Oral sertraline raised the 2-min unmetabolized ^{11}C -DASB percentage. **Conclusion:** Measurement and fitting of early metabolism time points improves curve fitting, significantly affects volume-of-distribution determination, and improves test-retest reproducibility. Saturation of lung 5-HT transporters by sertraline prevents the initial trapping of ^{11}C -DASB. Initial trapping of high-affinity radioligands may be important in the quantification of the binding of other ligands with a high concentration of binding sites in the lungs.

Key Words: 5-HT; lung; modeling

J Nucl Med 2006; 47:1796-1802

The serotonin (5-hydroxytryptamine, or 5-HT) transporter is the primary target for selective serotonin reuptake inhibitors (SSRIs). SSRIs are an effective treatment for major depressive disorder, obsessive compulsive disorder, post-traumatic stress disorder, generalized anxiety disorder, and other mood and anxiety disorders (1). SSRIs bind to the transporter, blocking the reuptake of 5-HT, and stimulate a chain of intracellular events including desensitization of 5-HT_{1A} autoreceptors, increases in neuronal firing rate, and downstream trophic effects that are temporally associated with clinical response (2,3). In vivo imaging studies report less 5-HT transporter binding in the midbrain (4,5) and amygdala in major depression (5). PET studies have reported on the relationship of 5-HT transporter occupancy in vivo to oral doses and plasma levels of SSRIs (6-8).

^{11}C -3-Amino-4-(2-dimethylaminomethylphenylsulfanyl)benzotrile (DASB) binds with high affinity (1.1 nmol/L) and selectivity to the 5-HT transporter and offers advantages over other PET 5-HT transporter radioligands (6,9-12). During the course of our determination of the optimal region of interest and voxel-based modeling methods for quantifying 5-HT transporter binding using PET and ^{11}C -DASB (13), we observed that the initial metabolite point (the percentage of unmetabolized ^{11}C -DASB) was lower at the 2-min time point than at the 12-min time point, a phenomenon we have not observed with other radioligands (Fig. 1A) (14,15). Also, a 1-tissue-compartment model did not adequately describe the rising portion of the time-activity curve (Fig. 2A). Because the lung is the critical organ for ^{11}C -DASB (16) and the tracer is injected intravenously, making its first pass through the pulmonary vasculature, one explanation of this phenomenon is that the unmetabolized ^{11}C -DASB is "trapped," briefly, in the lung.

In dogs, the lungs take up at least 90% of plasma 5-HT and are considered a site of 5-HT reuptake from the blood (17). In the human lung, the maximal concentration of 5-HT transporter is 7.50 pmol/mg of protein (18), a concentration

Received Apr. 5, 2006; revision accepted Aug. 14, 2006.
For correspondence contact: Ramin V. Parsey, MD, PhD, New York State Psychiatric Institute, 1051 Riverside Dr., Box 42, New York, NY 10032.
E-mail: rparsey@neuron.cpmc.columbia.edu
COPYRIGHT © 2006 by the Society of Nuclear Medicine, Inc.

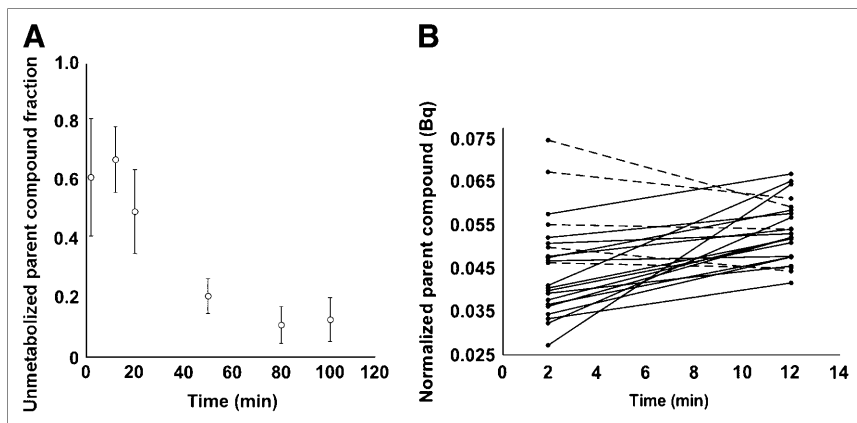


FIGURE 1. (A) Average unmetabolized ^{11}C -DASB fraction vs. time for baseline studies. Unlike other ligands, fraction is lower at first time point (2 min) than at second time point (12 min). (B) This lower fraction is caused by lower level of unmetabolized parent compound at 2 min than at 12 min (solid lines) in all but 5 studies (dashed lines).

that is at least an order of magnitude greater than the maximal concentration of 5-HT transporters in the dorsal raphe nucleus, 329 fmol/mg of tissue (19). In addition, SSRIs such as fluoxetine and venlafaxine have been reported to accumulate in the lungs of mice (20) and humans (21).

In this study, we examined 2 modeling methods to fit this unique unmetabolized fraction curve, and we assessed their impact on the quantification and reproducibility of ^{11}C -DASB binding in the brain. We also tested the effect of prior administration of an SSRI, sertraline, to block the lung sites and determine whether there is an effect on ^{11}C -DASB metabolism.

MATERIALS AND METHODS

Subjects

Healthy volunteers were recruited for the study. Inclusion criteria were assessed by the following: history, Structured Clinical Interview for DSM-IV (22), review of systems, physical examination, routine blood tests, pregnancy test, urine toxicology, and electrocardiography. Inclusion criteria included an age between 18 and 65 y, absence of any axis I DSM-V psychiatric diagnoses, absence of any medications for at least 2 wk, absence of a lifetime history of alcohol or substance abuse or dependence, absence of a lifetime exposure to 3,4-methylenedioxymethamphetamine (“ecstasy”), absence of significant medical conditions, absence of pregnancy, and capacity to provide informed consent.

The Institutional Review Boards of Columbia University Medical Center and the New York State Psychiatric Institute approved the protocol. Subjects gave written informed consent after receiving an explanation of the study. Eleven subjects were enrolled in the study (4 men and 7 women; mean age \pm SD, 27 ± 6 y; range, 18–36 y). All subjects underwent 2 identical scans, test–retest, on the same day. Six subjects had occupancy scans taken after 2 d of receiving 50 mg/d and then after 4 d of receiving 100 mg/d of sertraline. These subjects were part of a larger study of 5-HT transporter occupancy (8) and model determination (13).

Radiochemistry

^{11}C -DASB was prepared as previously described (23). The chemical purity of ^{11}C -DASB was greater than 99%, and the radiochemical purity was greater than 90%. The mean specific activity at injection was 55.5 MBq/nmol, and the mean injected dose was 570 ± 104 MBq.

PET Protocol

A venous catheter was used for injection of the radiotracer, and an arterial catheter was used to obtain samples for the input function. A polyurethane head-holder system (Soule Medical) was molded around the subject’s head for immobilization. PET was performed with an ECAT HR+ (Siemens/CTI). A 10-min transmission scan was obtained before radiotracer injection. At the end of the transmission scan, between 185 and 740 MBq of ^{11}C -DASB were administered intravenously as a bolus over 30 s. Emission data were collected in 3-dimensional mode for 120 min using 21

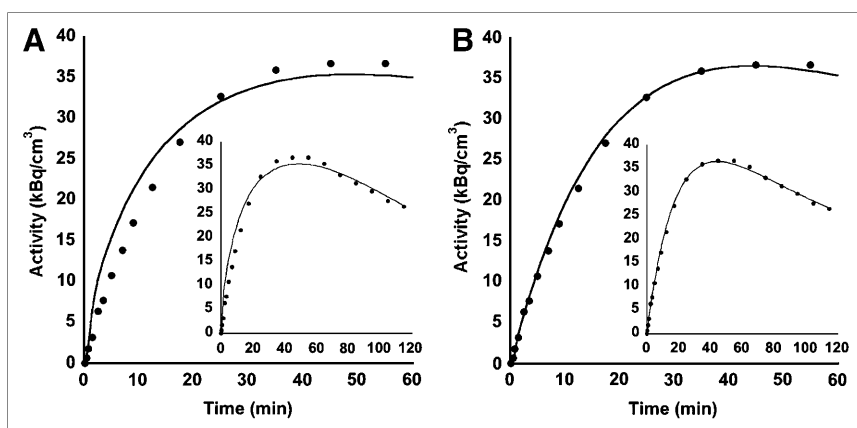


FIGURE 2. Time–activity curves for amygdala using ND – 1 (A) and power-function–damped (B) metabolite fits. Time–activity curve fitting using ND – 1 metabolite curve fitting is clearly inadequate for early time points. Data are truncated at 60 min; full datasets are shown in insets.

frames of increasing duration: 3 at 20 s, 3 at 1 min, 3 at 2 min, 2 at 5 min, and 10 at 10 min. Images were reconstructed to a 128 × 128 matrix (pixel size, 2.5 × 2.5 mm). Reconstruction was performed with attenuation correction using the transmission data, and scatter was corrected using a model-based method (24). The reconstruction filter and estimated image filter were Shepp 0.5 (2.5 mm in full width at half maximum), the Z filter was all-pass 0.4 (2.0 mm in full width at half maximum), and the zoom factor was 4.0, leading to a final image resolution of 5.1 mm in full width at half maximum at the center of the field of view (25).

Input Function Measurement

Arterial samples were collected by an automated sampling system every 5 s for the first 2 min and manually thereafter for a total of 31 samples. Centrifuged plasma samples were collected in 200- μ L aliquots, and the radioactivity was measured in a well counter. A high-pressure liquid chromatography assay of 6 samples (collected at 2, 12, 20, 50, 80, and 100 min) provided unmetabolized parent and metabolite compound levels. The supernatant liquid obtained after centrifugation of the blood sample at 2,000 rpm for 1 min was transferred (0.5 mL) into a tube and mixed with acetonitrile (0.7 mL). The resulting mixture was stirred with a vortex mixer for 10 s and centrifuged at 14,000 rpm for 4 min. Approximately 0.2 mL of supernatant was removed, and radioactivity was measured in a well counter; 0.8 mL was injected onto the high-pressure liquid chromatography column (Phenomenex Prodigy C18 ODS [10 × 250 mm, 10 μ m]; mobile phase, 50:50 acetonitrile:water 0.1 mol/L ammonium formate; flow rate, 5 mL/min; retention time of 11 C-DASB, \sim 7 min). The metabolite and unmetabolized parent compound were collected in separate vials, and radioactivity was quantified using a Bioscan γ -detector after correction for background radioactivity. To ensure the retention time of the parent fraction, we injected corresponding quality control and standard samples at the beginning and end of the study. We calculated unmetabolized parent fraction as the activity in the parent vial divided by the parent plus metabolite vials. In addition, we measured total parent radioactivity and, to facilitate comparison across subjects, normalized to the total radioactivity injected in the high-pressure liquid chromatography column (Fig. 1B). The 6 unmetabolized parent fraction levels were fit with equations described in the following section. The input function was calculated as the product of the interpolated parent fraction and the total plasma counts. After fitting a straight line between time zero and the peak of the input function, subsequent time points of the measured input function values were fitted to a sum of 3 exponentials, and the fitted values were used as input to the analyses.

Metabolite Curve Fitting

For the first 2 models, the unmetabolized fraction data are fit with a sum of 2 exponentials with coefficients constrained so that the function is 1 at time zero. The smaller of the 2 time constants of the 2 exponentials is constrained to equal the difference between $\lambda_{\text{cerebellum}}$, the terminal rate of washout of cerebellar activity, and λ_{total} , the smallest elimination rate constant of the total plasma (26):

$$f(t) = Ce^{-\lambda_1 t} + (1 - C)e^{-\lambda_{\text{cal}} t},$$

where λ_{cal} is the calculated time constant ($\lambda_{\text{cal}} = \lambda_{\text{cerebellum}} - \lambda_{\text{total}}$) and C and λ_1 are estimated from the data. This baseline model is

referred to as the no-damping (ND) model. The model with the first metabolite point removed is referred to as ND - 1.

Because this model dictates that the unmetabolized portion begins at 1 and decreases monotonically thereafter, it does not adequately account for early trapping of the compound in the lung. We propose to account for this effect by multiplying the baseline model by a term that will damp the early times. We used a power function for this purpose and dropped the constraint that the sum of the coefficients of the exponentials is 1:

$$f(t) = t^\alpha (C_1 e^{-\lambda_1 t} + C_2 e^{-\lambda_{\text{cal}} t}).$$

For small values of t , the power function dominates and $f(t)$ is near zero. As t increases, the exponential portions dominate the power function. Thus, $f(t)$ decays toward zero as t increases, as we would predict. This increases the number of model parameters by 2. We call this the power-function-damped model.

Metabolite models are fit using standard nonlinear least-squares methodology with weights derived from SE values returned from the γ -counter used in metabolite analysis.

MRI

MR images were acquired on a 1.5-T Signa Advantage system (GE Healthcare). A sagittal scout image (localizer) was obtained to identify the anterior commissure–posterior commissure plane (1 min), followed by a transaxial T1-weighted sequence with a 1.5-mm slice thickness in a coronal plane orthogonal to the anterior commissure–posterior commissure plane over the entire brain. The parameters were as follows: 3-dimensional spoiled gradient-recalled acquisition in the steady state; repetition time, 34 ms; echo time, 5 ms; flip angle, 45°; slice thickness, 1.5 mm with no gap; 124 slices; field of view, 22 × 16 cm; matrix, 256 × 192 reformatted to 256 × 256, yielding a voxel size of 1.5 × 0.9 × 0.9 mm; and time of acquisition, 11 min.

Image Analysis

Images were analyzed using MEDX software (Sensor Systems, Inc.). The last 13 frames of an individual study were coregistered to the eighth frame using a tool available from the Oxford Centre for Functional Magnetic Resonance Imaging of the Brain (FMRIB)—the FMRIB linear image registration tool (FLIRT), version 5.0 (27)—to correct for patient motion during the scan. A mean motion-corrected PET image was created and coregistered to its corresponding MR image using FLIRT. The resulting transformation was applied to all motion-corrected frames. Regions of interest were traced on the basis of brain atlases (28,29) and published reports (30,31) and included the anterior cingulate, cingulate cortex, amygdala, hippocampus, insular cortex, temporal cortex, dorsal caudate, midbrain, ventral striatum, thalamus, dorsal putamen, dorsolateral prefrontal cortex, occipital cortex, orbital prefrontal cortex, entorhinal cortex, cerebellar gray matter, medial prefrontal cortex, parietal lobe, parahippocampal gyrus, and posterior parahippocampal gyrus. MR images were cropped using the Exbrain utility (version 2; UCL Institute of Neurology (32)) and then segmented using the FMRIB automated segmentation tool (33). Within the cortex, only gray matter voxels were used to measure the PET activity distribution. Regions of interest were drawn by 3 different data analysts who were unaware of the condition. Test–retest variability in the volume of distribution (V_T) between the 3 raters over all regions of interest was less than 3%.

Outcome Measures

Several methods for the quantification of ^{11}C -DASB binding have been described (12,34,35). In this article, ^{11}C -DASB regional V_T values were derived using a 1-tissue-compartment model and likelihood estimation in the graphical approach, which reduces the noise-dependent bias inherent in the graphical approach (36–38). The 1-tissue-compartment configuration included the arterial plasma compartment (C_a) and 1 tissue compartment (C_T) that included the intracerebral free, nonspecifically bound, and specifically bound compartments. Brain activity was corrected for the contribution of plasma activity assuming a 5% blood volume in the regions of interest (39).

The total regional V_T (mL of plasma/g of tissue) was defined as the ratio of the tracer concentration in this region to the metabolite-corrected plasma concentration at equilibrium:

$$V_T = \frac{C_T}{C_a}$$

Kinetic derivations of total V_T were obtained as

$$V_T = \frac{K_1}{k_2'}$$

where K_1 ($\text{mL}\cdot\text{g}^{-1}\cdot\text{min}^{-1}$) is the unidirectional fractional rate constants for the transfer between C_a and C_T , and k_2' (min^{-1}) is the fractional rate constant for the transfer from C_T to C_a (14).

Statistics

V_T values estimated using the different metabolite models were compared using a linear mixed-effects model on $\log(V_T)$ with subject and scan (nested within subject) as random effects and region and metabolite model as fixed effects. The log transform was used to approximately equalize the variance among regions.

RESULTS

Generally, when a tracer is administered to a subject as a bolus, the entirety of the compound initially injected is the original, or parent, compound, and the compound is metabolized over time. With ^{11}C -DASB, we observed in 77%

of the studies that the first metabolite point, at 2 min, indicated less unmetabolized parent fraction (Fig. 1A) than did the next time point, at 12 min. This finding was due to a lower level of total unmetabolized parent at the 2-min time point in all but 5 studies (Fig. 1B). Fitting the change in percentage of unmetabolized parent compound as a function of time with the sum of 2 exponentials (ND), as is routinely done with this ligand (12) and other 5-HT transporter ligands (14), insufficiently describes this metabolism time course (Fig. 3A). Instead we used 2 alternative methods. In all cases, the terminal portion of the metabolite curve is described by the sum of 2 exponentials where the time constant of the second exponential is constrained. In the alternative methods, we either remove the first time point and fit the remaining points with ND (ND – 1, Fig. 3B) or describe the rising portion of the curve with power function damping (Fig. 3C). Power function damping has the lowest weighted residuals at each time point relative to the ND – 1 (Fig. 4).

We then explored whether the improved fitting of the metabolite data by the power-function-damped method made any difference in outcome measures. We used a 1-tissue-compartment model to determine the V_T and found that without a damping function (ND – 1), V_T is underestimated relative to power function damping ($F_{1,838} = 545$, $P < 0.0001$; Fig. 5A) but in very close agreement with other groups ($r^2 = 0.99$ compared with the findings of Frankle et al. (12)). A similar underestimation was observed if we used likelihood estimation in the graphical approach to model the data ($F_{1,838} = 801$, $P < 0.0001$; Fig. 5B). The mean test–retest reproducibility (measured as the difference between the 2 observations divided by the mean across all regions) is also improved by using power function damping ($5.9\% \pm 2.5\%$) instead of ND – 1 ($10.9\% \pm 9.1\%$). Similar results were obtained using likelihood estimation in the graphical approach ($5.7\% \pm 1.2\%$ [power function damping] vs. $9.5\% \pm 10.4\%$ [ND – 1]).

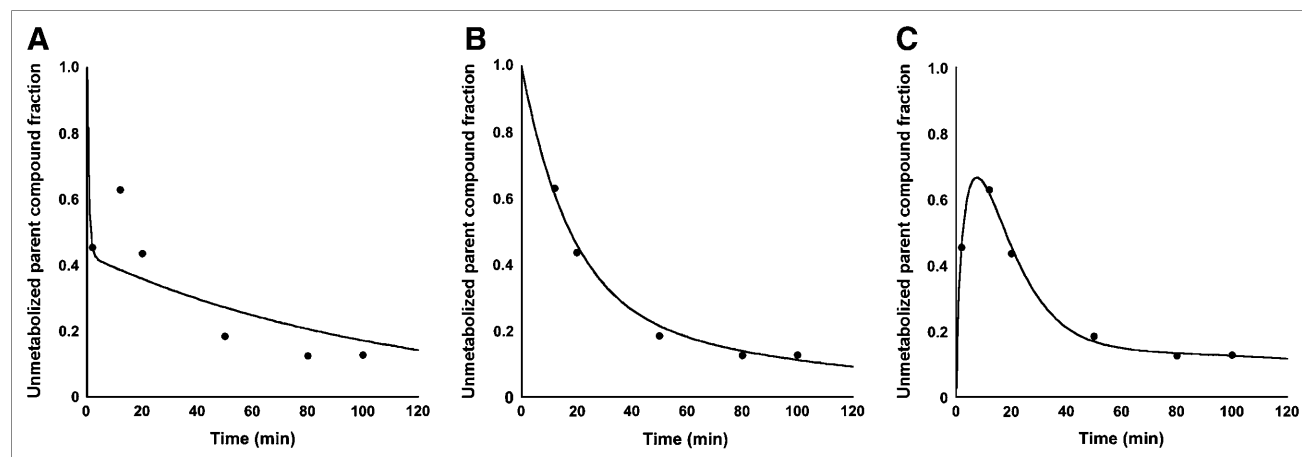


FIGURE 3. Unmetabolized ^{11}C -DASB fraction vs. time data (circles) fit with ND (A), ND with first metabolite point removed (B), and power-function-damped (C) metabolite fits (lines) for study. ND is clearly inadequate for fitting and will not be used in subsequent analyses.

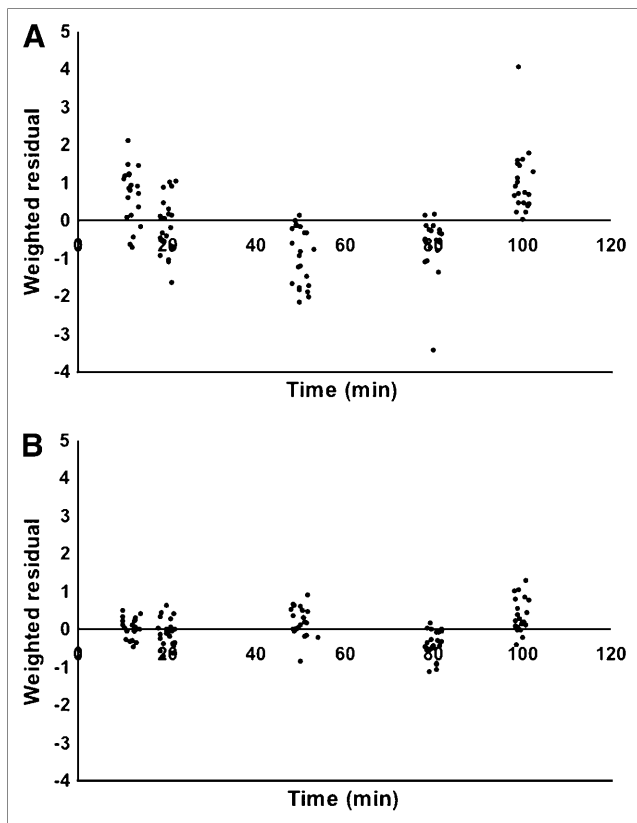


FIGURE 4. Graph of weighted residuals vs. time for each metabolite fit, jittered on time axis. Metabolite data were fit with ND - 1 (A) and power-function-damped (B) models.

If the large number of 5-HT transporters in the lungs are acting as a trap for the initial intravenous bolus injection of ^{11}C -DASB, then pretreating subjects with high doses of an SSRI such as sertraline could ameliorate this initial trapping. Metabolite curves for subjects in our previous study, who had plasma sertraline levels greater than or equal to 13 ng/mL, are shown in Figure 6. In these subjects, the 2-min time point is lower than the 12-min time point on baseline scan days (Fig. 6A). In scans performed when these subjects were treated with sertraline, the unmetabo-

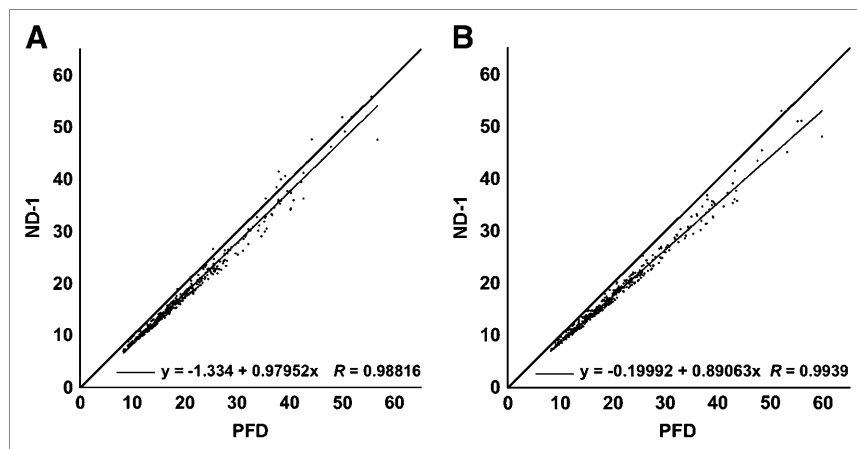
lized parent fraction at 2 min is higher than the 12-min time point (Fig. 6B; $P = 0.015$).

DISCUSSION

We have shown that a power-function-damped 2-exponential fit describes ^{11}C -DASB metabolite data, resulting in both higher V_T determinations and improved test-retest reproducibility. An ^{11}C -DASB injection in the presence of high plasma levels of sertraline raises the unmetabolized fraction at the 2-min time point. This finding supports the hypothesis that the large number of 5-HT transporter binding sites in the lung transiently traps the 5-HT transporter radioligand ^{11}C -DASB after it is intravenously injected as a bolus. Conversely, the ^{11}C -DASB metabolite lacks affinity for 5-HT transporter and is not delayed in passage through the lungs. As can be seen in Figure 2 of Lu et al. (16), over 50% of the injected dose of ^{11}C -DASB in humans is in the lungs at initial time points, compared with just slightly over 5% in the organ with the next highest uptake, the heart. Uptake in the brain does not peak until approximately 15 min after injection.

Only one other ^{11}C -DASB study measured metabolites at 2 min (12). Although that study found a larger SD at the 2-min time point than at the other time points, the mean was greater than that at the 12-min time point. That initial publication involved only 6 subjects, and most subjects since then have had lower 2-min metabolite points (Gordon Frankle, oral communication, 2006). All other groups quantifying 5-HT transporter with ^{11}C -DASB either have not had arterial input data or have measured metabolites starting at 5 min. We found that fitting the metabolite data with all data points with ND or fitting the data without the 2-min data point (ND - 1) underestimated V_T compared with power function damping (the slope was 0.89 for ND - 1 V_T vs. power-function-damped V_T and 0.83 for ND V_T vs. power-function-damped V_T). Although several alternative models for describing the metabolite curve were considered, we could see no room for improvement in the fitting by power function damping and do not present the data.

FIGURE 5. Comparison of V_T values with power-function-damped (PFD) metabolite fit against those determined with ND - 1 using 1-tissue-compartment model (A) and likelihood estimation in graphical approach (B). All regions of interest for all studies are plotted. Line is identity. An outlier is excluded from both graphs.



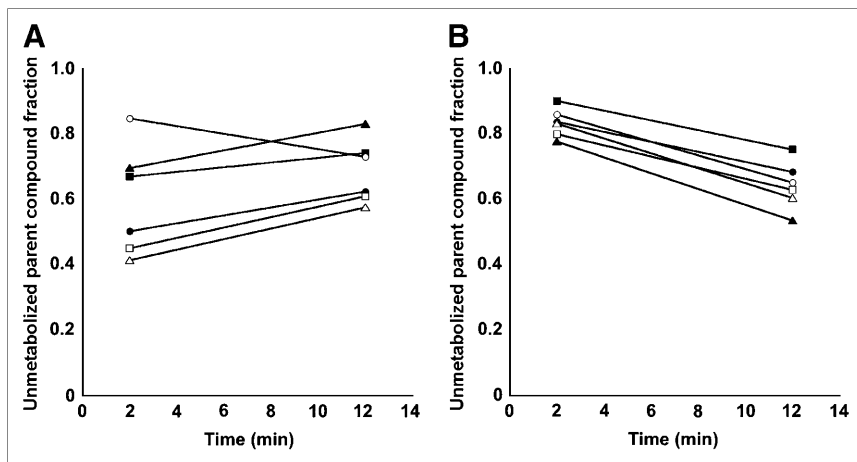


FIGURE 6. Plots of unmetabolized ^{11}C -DASB vs. time for same subjects on baseline scan days (A) and occupancy scan days (B). Subjects had plasma sertraline level ≥ 13 ng/mL on day of occupancy study. On baseline days, most subjects had lower unmetabolized ^{11}C -DASB at 2 min than at 12 min. After subjects received saturating doses of sertraline, pattern was reversed. Subjects are identified with unique markers.

This metabolite pattern has not been observed with other PET ligands in humans, such as ^{11}C -labeled hexahydro-6-[4-(methylthio)phenyl]pyrrolo[2,1-a]isoquinoline (McN5652) (14), ^{11}C -labeled 2-(2-((dimethylamino)methyl)phenylthio)-5-methylaniline (MADAM) (40), and ^{123}I -labeled 2-(2-((dimethylamino)methyl)phenylthio)-5-iodoaniline (ADAM) (41), possibly because of slower initial metabolism or slight differences in affinity.

Although analytic high-pressure liquid chromatography columns are widely used for the analysis of metabolites, we have used a semipreparative column for ^{11}C -DASB as has been done in the past with other compounds (42–44). With an analytic column (Phenomenex Prodigy C18 ODS), a significant difference in the retention time of the parent compound with respect to standard ^{11}C -DASB was observed. With a semipreparative column, the retention time of the parent agreed with that of standard ^{11}C -DASB (7–8 min).

One consequence of using power function damping to fit the metabolite data is that the initial rise of the time–activity curve is better fit by the model. Effectively, this improvement is due to higher K_1 values; our range was between 0.25 and 0.95 mL/min/g, compared with 0.62–0.81 mL/min/g as described by Ginovart et al. (34). Because K_1 is the product of extraction and blood flow, K_1 can never be greater than blood flow. Assuming an extraction of 1, none of our K_1 values across any region of interest was above a generally acceptable blood flow value of 1.07 mL/min/g (45).

If correct, our hypothesis regarding initial lung trapping of a radioligand could affect other radioligands for binding sites that have a high concentration of their target in the lungs, such as the 5-HT_{2A} system; our dosimetry studies in baboons suggest that, like the 5-HT transporter, this system has the lung as the critical organ as well (data not shown).

CONCLUSION

Although we have suggested one possible cause for the atypical metabolism of ^{11}C -DASB—selective trapping of

the parent compound by the large number of 5-HT transporters in the lungs—we realize other explanations are possible. Regardless of the biologic cause, careful examination and fitting of the rate of metabolism of radioligands can improve the fitting of time–activity curves and the reproducibility of outcome measures and should be applied to previously acquired data as well as to future studies using this ligand.

ACKNOWLEDGMENTS

We thank the employees of the Brain Imaging Core of the NIMH-funded Conte Translational Neuroscience Center, the Kreitchman PET Center, and the Columbia University Radioligand Laboratory for expert help. This work was supported in part by an investigator-initiated grant from Pfizer Inc.

REFERENCES

- Shelton RC. The dual-action hypothesis: does pharmacology matter? *J Clin Psychiatry*. 2004;65(suppl 17):5–10.
- Blier P, de Montigny C. Serotonin and drug-induced therapeutic responses in major depression, obsessive-compulsive and panic disorders. *Neuropsychopharmacology*. 1999;21(2 suppl):91S–98S.
- Duman RS, Heninger GR, Nestler EJ. A molecular and cellular theory of depression. *Arch Gen Psychiatry*. 1997;54:597–606.
- Malison RT, Price LH, Berman R, et al. Reduced brain serotonin transporter availability in major depression as measured by [^{123}I]-2 beta-carbomethoxy-3 beta-(4-iodophenyl)tropane and single photon emission computed tomography. *Biol Psychiatry*. 1998;44:1090–1098.
- Parsey RV, Hastings RS, Oquendo MA, et al. Lower serotonin transporter binding potential in the human brain during major depressive episodes. *Am J Psychiatry*. 2006;163:52–58.
- Meyer JH, Wilson AA, Ginovart N, et al. Occupancy of serotonin transporters by paroxetine and citalopram during treatment of depression: a [(11)C]DASB PET imaging study. *Am J Psychiatry*. 2001;158:1843–1849.
- Meyer JH, Wilson AA, Sagrati S, et al. Serotonin transporter occupancy of five selective serotonin reuptake inhibitors at different doses: an [(11)C]DASB positron emission tomography study. *Am J Psychiatry*. 2004;161:826–835.
- Parsey RV, Kent JM, Oquendo MA, et al. Acute occupancy of brain serotonin transporter by sertraline as measured by [^{11}C]DASB and positron emission tomography. *Biol Psychiatry*. 2006;59:821–828.
- Wilson AA, Ginovart N, Schmidt M, Meyer JH, Threlkeld PG, Houle S. Novel radiotracers for imaging the serotonin transporter by positron emission tomography:

- synthesis, radiosynthesis, and in vitro and ex vivo evaluation of (11)C-labeled 2-(phenylthio)araalkylamines. *J Med Chem.* 2000;43:3103–3110.
10. Wilson AA, Ginovart N, Hussey D, Meyer J, Houle S. In vitro and in vivo characterisation of [¹¹C]-DASB: a probe for in vivo measurements of the serotonin transporter by positron emission tomography. *Nucl Med Biol.* 2002;29:509–515.
 11. Houle S, Ginovart N, Hussey D, Meyer JH, Wilson AA. Imaging the serotonin transporter with positron emission tomography: initial human studies with [¹¹C]DAPP and [¹¹C]DASB. *Eur J Nucl Med.* 2000;27:1719–1722.
 12. Frankle WG, Huang Y, Hwang DR, et al. Comparative evaluation of serotonin transporter radioligands ¹¹C-DASB and ¹¹C-McN 5652 in healthy humans. *J Nucl Med.* 2004;45:682–694.
 13. Ogden RT, Ojha A, Erlandsson K, Oquendo MA, Mann JJ, Parsey RV. In vivo quantification of serotonin transporters using [¹¹C]DASB and positron emission tomography in humans: modeling considerations. *J Cereb Blood Flow Metab.* May 17, 2006 [Epub ahead of print].
 14. Parsey RV, Kegeles LS, Hwang DR, et al. In vivo quantification of brain serotonin transporters in humans using [¹¹C]McN 5652. *J Nucl Med.* 2000;41:1465–1477.
 15. Parsey RV, Slifstein M, Hwang DR, et al. Validation and reproducibility of measurement of 5-HT1A receptor parameters with [carbonyl-¹¹C]WAY-100635 in humans: comparison of arterial and reference tissue input functions. *J Cereb Blood Flow Metab.* 2000;20:1111–1133.
 16. Lu JQ, Ichise M, Liow JS, Ghose S, Vines D, Innis RB. Biodistribution and radiation dosimetry of the serotonin transporter ligand ¹¹C-DASB determined from human whole-body PET. *J Nucl Med.* 2004;45:1555–1559.
 17. Thomas DP, Vane JR. 5-hydroxytryptamine in the circulation of the dog. *Nature.* 1967;216:335–338.
 18. Morin D, Zini R, Lange J, Tillement JP. Evidence for high affinity [³H] imipramine binding sites in human lung. *Biochem Biophys Res Commun.* 1984;120:926–932.
 19. Arango V, Underwood MD, Boldrini M, et al. Serotonin 1A receptors, serotonin transporter binding and serotonin transporter mRNA expression in the brainstem of depressed suicide victims. *Neuropsychopharmacology.* 2001;25:892–903.
 20. Shiue CY, Shiue GG, Cornish KG, O'Rourke MF. PET study of the distribution of [¹¹C]fluoxetine in a monkey brain. *Nucl Med Biol.* 1995;22:613–616.
 21. Malizia AL, Melichar JM, Brown DJ, et al. Demonstration of clomipramine and venlafaxine occupation at serotonin reuptake sites in man in vivo. *J Psychopharmacol.* 1997;11:279–281.
 22. First MB Sr, Gibbon M, Williams JBW. *Structured Clinical Interview for DSM-IV Axis I Disorders.* Washington, DC: American Psychiatric Press; 1997.
 23. Belanger MJ, Simpson NR, Wang T, Van Heertum R, Mann JJ, Parsey RV. Biodistribution and radiation dosimetry of [¹¹C]DASB in baboons. *Nucl Med Biol.* 2004;31:1097–1102.
 24. Watson CC, Newport D, Casey ME. *A Single Scatter Simulation Technique for Scatter Correction in 3D PET.* Dordrecht, The Netherlands: Kluwer Academic Publishers; 1996.
 25. Mawlawi O, Martinez D, Slifstein M, et al. Imaging human mesolimbic dopamine transmission with positron emission tomography: I. Accuracy and precision of D(2) receptor parameter measurements in ventral striatum. *J Cereb Blood Flow Metab.* 2001;21:1034–1057.
 26. Abi-Dargham A, Simpson N, Kegeles L, et al. PET studies of binding competition between endogenous dopamine and the D1 radiotracer [¹¹C]NNC 756. *Synapse.* 1999;32:93–109.
 27. Jenkinson M, Smith S. A global optimisation method for robust affine registration of brain images. *Med Image Anal.* 2001;5:143–156.
 28. Duvernoy H. *The Human Brain: Surface, Three-Dimensional Sectional Anatomy and MRI.* New York, NY: Springer-Verlag Wien; 1991.
 29. Talairach J, Tournoux P. *Co-Planar Stereotaxic Atlas of the Human Brain: Three-Dimensional Proportional System—An Approach of Cerebral Imaging.* New York, NY: Thieme Medical Publisher; 1988.
 30. Kates WR, Abrams MT, Kaufmann WE, Breiter SN, Reiss AL. Reliability and validity of MRI measurement of the amygdala and hippocampus in children with fragile X syndrome. *Psychiatry Res.* 1997;75:31–48.
 31. Killiany RJ, Moss MB, Nicholson T, Jolesz F, Sandor T. An interactive procedure for extracting features of the brain from magnetic resonance images: the lobes. *Hum Brain Mapp.* 1997;5:355–363.
 32. Lemieux L, Hammers A, Mackinnon T, Liu RS. Automatic segmentation of the brain and intracranial cerebrospinal fluid in T1-weighted volume MRI scans of the head, and its application to serial cerebral and intracranial volumetry. *Magn Reson Med.* 2003;49:872–884.
 33. Smith SM, Jenkinson M, Woolrich MW, et al. Advances in functional and structural MR image analysis and implementation as FSL. *Neuroimage.* 2004;23(suppl 1):S208–S219.
 34. Ginovart N, Wilson AA, Meyer JH, Hussey D, Houle S. Positron emission tomography quantification of [(11)C]-DASB binding to the human serotonin transporter: modeling strategies. *J Cereb Blood Flow Metab.* 2001;21:1342–1353.
 35. Ichise M, Liow JS, Lu JQ, et al. Linearized reference tissue parametric imaging methods: application to [¹¹C]DASB positron emission tomography studies of the serotonin transporter in human brain. *J Cereb Blood Flow Metab.* 2003;23:1096–1112.
 36. Ogden RT. On estimation of kinetic parameters in graphical analysis of PET imaging data. *Stat Med.* 2003;22:3557–3568.
 37. Ogden RT, Parsey RV, Mann JJ. Likelihood approach to parameter estimation in Logan graphical analysis [abstract]. *Neuroimage.* 2002;16(suppl):S73.
 38. Parsey RV, Ogden RT, Mann JJ. Determination of volume of distribution using likelihood estimation in graphical analysis: elimination of estimation bias. *J Cereb Blood Flow Metab.* 2003;23:1471–1478.
 39. Mintun MA, Raichle ME, Kilbourn MR, Wooten GF, Welch MJ. A quantitative model for the in vivo assessment of drug binding sites with positron emission tomography. *Ann Neurol.* 1984;15:217–227.
 40. Lundberg J, Odano I, Olsson H, Halldin C, Farde L. Quantification of ¹¹C-MADAM binding to the serotonin transporter in the human brain. *J Nucl Med.* 2005;46:1505–1515.
 41. Catafau AM, Perez V, Penengo MM, et al. SPECT of serotonin transporters using ¹²³I-ADAM: optimal imaging time after bolus injection and long-term test-retest in healthy volunteers. *J Nucl Med.* 2005;46:1301–1309.
 42. Schou M, Halldin C, Sovago J, et al. Specific in vivo binding to the norepinephrine transporter demonstrated with the PET radioligand, (S,S)-[¹¹C]MeNER. *Nucl Med Biol.* 2003;30:707–714.
 43. Kumar JS, Majo VJ, Hsiung SC, et al. Synthesis and in vivo validation of [O-methyl-¹¹C]-2-[4-[4-(7-methoxynaphthalen-1-yl)piperazin-1-yl]butyl]-4-methyl-2H-[1,2,4]triazine-3,5-dione: a novel 5-HT1A receptor agonist positron emission tomography ligand. *J Med Chem.* 2006;49:125–134.
 44. Goethals P, van Eijkeren M, Lodewyck W, Dams R. Measurement of [methyl-carbon-11]thymidine and its metabolites in head and neck tumors. *J Nucl Med.* 1995;36:880–882.
 45. Law I, Iida H, Holm S, et al. Quantitation of regional cerebral blood flow corrected for partial volume effect using O-15 water and PET: II. Normal values and gray matter blood flow response to visual activation. *J Cereb Blood Flow Metab.* 2000;20:1252–1263.